Published in final edited form as:
NMR Biomed. 2009 June ; 22(5): 480–487. doi:10.1002/nbm.1358.

The MT pool size ratio and the DTI radial diffusivity may reflect the myelination in shiverer and control mice

Xiawei Ou[a,b,c,*], **Shu-Wei Sun**[d], **Hsiao-Fang Liang**[d], **Sheng-Kwei Song**[d], and **Daniel F. Gochberg**[a]

[a]Department of Radiology, Vanderbilt University Institute of Imaging Science, Nashville, TN 37232, USA

[b]Radiology Department, Arkansas Children's Hospital, Little Rock, AR 72202, USA

[c]Department of Radiology, University of Arkansas for Medical Sciences, Little Rock, AR 72205, USA

[d]Department of Radiology, Washington University School of Medicine, St. Louis, MO 63110, USA

Abstract

A quantitative magnetization transfer (qMT) technique was employed to quantify the ratio of the sizes of the bound and free water proton pools in *ex vivo* mouse brains. The goal was to determine the pool size ratio sensitivity to myelin. Fixed brains from both shiverer mice and control littermates were imaged. The pool size ratio in the corpus callosum of shiverer mice was substantially lower than that in the control mice, while there was no distinguishable difference in the pool size ratio in the gray matter. These results correlate with diffusion tensor imaging (DTI) derived radial diffusivity which previously was shown to reflect myelin integrity in this animal model. Histological study reveals the presence of myelin in control mice white matter and the absence of myelin in shiverer mice white matter, supporting the qMT and DTI results. Our findings support the view that qMT may be used for estimating myelin integrity.

Keywords

quantitative magnetization transfer; pool size ratio; diffusion tensor imaging; radial diffusivity; corpus callosum; myelin

INTRODUCTION

Myelin damage is an important pathological feature in many central nervous system (CNS) disorders, such as multiple sclerosis (MS) (1,2). Magnetic resonance techniques provide useful non-invasive measures of the pathology in MS (3). Conventional MRI techniques have played significant roles in white matter lesion (WML) detection in the clinical and research settings. Though sensitive to demyelination, many of these MR techniques are also affected by other white matter pathologies, such as edema, inflammation, and axonal degeneration (4,5). In contrast, the macromolecular pool size ratio obtained by quantitative magnetization transfer (qMT) imaging (6–8), the radial diffusivity obtained by diffusion

[*]Correspondence to: X. Ou, Arkansas Children's Hospital, 800 Marshall St, Slot 105, Little Rock, AR 72202, USA. ouxiawei@uams.edu.

tensor imaging (DTI) (9), and the myelin water fraction obtained by multiple T_2 measurements (10–12), potentially provide more specific measures of myelin integrity.

qMT is a quantitative description of magnetization transfer (MT), which is the exchange of magnetization between macromolecular protons (such as protons in myelin sheaths) and free protons (such as protons in tissue water). Conventional MT imaging is produced by applying an off-resonance pulse to selectively saturate the macromolecular protons and measuring the change in the free water magnetization. One parameter generally used to characterize MT is the magnetization transfer ratio (MTR), which is defined by MTR = $(1 - S/S_0) \times 100\%$, where S and S_0 represent the signal with and without the saturation pulse, respectively. MTR values have been shown to be smaller in MS lesions than in normal white matter, and may be an indirect reflection of myelin (3). However, MTR is not a simple measure of demyelination; it is also affected by other changes. For example, MTR decreases with inflammation (5). Furthermore, MTR values are highly dependent on pulse sequence timings, rf pulse shapes, and B_1 variations, making comparisons between results from different research sites difficult (13).

MTR values are a function of both relaxation and exchange and are therefore difficult to interpret in terms of the underlying biological process. In contrast, qMT provides a more specific description of MT by measuring the relaxation times of each pool of protons, the exchange rates between pools, and the ratio of the pool sizes. qMT parameters have been measured in normal brains and different disease models to investigate the sensitivity to myelin. qMT measurements showed that pool size ratios are greater in white matter than in gray matter (14), and smaller in MS lesions than in normal white matter (8), suggesting that pool size ratio is capable of reflecting myelin contents. In addition, normal appearing white matter (NAWM) in MS patients was studied by both MTR and qMT, and the results indicate that the qMT measured pool size ratio has a greater sensitivity in detecting myelin loss (6).

There are several published qMT techniques which yield either all or a subset of the relaxation and exchange parameters (15–19). Selective inversion recovery fast-spin-echo (SIR-FSE) is a qMT technique that selectively inverts the free pool magnetization and fits the resulting recovery to a bi-exponential function of the inversion time (20,21). We chose this method over the more widely applied pulsed saturation qMT method due to the easy implementation and data analysis of SIR-FSE. A more thorough discussion of the relative merits of the two methods is given elsewhere (20).

DTI is also widely used in studies of white matter diseases. While the summary parameters such as the apparent diffusion coefficient, the relative anisotropy, and the fractional anisotropy are reported to be different between MS lesions and normal white matter regions (22–24), none of these measures are capable of differentiating between the underlying axonal injury and demyelination. In contrast, the DTI derived directional diffusivities have demonstrated a much improved specificity. For example, DTI on mouse CNS has shown that the radial diffusivity (perpendicular to the axon fibers) is capable of detecting the presence of damage to myelin sheath in white matter, and the axial diffusivity (parallel to the axon fibers) detects the presence of injured axons in white matter (9,25–28).

Since both qMT and DTI may be capable of detecting myelin damage, imaging using both modalities on the same sample would provide confirmation of the myelin sensitivity, allow comparisons between the methods, and is potentially beneficial for the development of an optimized myelin marker. In this study, myelin pathology of CNS white matter tracts from the shiverer mouse, which lacks the myelin basic protein (MBP), will be examined. The myelin sheath in the CNS of shiverer mice is very thin, loose, or completely absent inmost of the cases (29,30). On the other hand, there is nearly no axon degeneration or

inflammation in shiverer mouse (31). Therefore, comparing shiverer mice to controls provides an excellent model to estimate the sensitivity of MR techniques to myelin integrity. Previous studies have used continuous wave (CW) and pulsed MT techniques to assess shiverer mice spinal cord (32) and used DTI techniques to assess the sensitivity and specificity of DTI to myelin integrity in shiverer mice brain (9). In the present study, a similar analysis was performed on the myelination of control/shiverer mice brain by using the SIR-FSE qMT method and comparing the results with DTI.

METHODS

Animal preparation

Six shiverer (6–8 week old, same type as used in the previous study (9), originally purchased from The Jackson Laboratory, Bar Harbor, Maine, USA) and six control mice (littermates) were euthanized and perfused with phosphate-buffered saline (PBS) followed by 10% formalin/PBS solution through the left cardiac ventricle. The mice were decapitated and their heads were kept in 10% formalin/PBS solution and stored at 4°C for 1 week. Before imaging, each mouse head was washed by PBS solution and then transferred to a 10 mm diameter cylinder filled with PBS solution.

Quantitative magnetization transfer imaging and diffusion tensor imaging

Each cylinder with a fixed number of mouse heads was placed in a 1 cm inner diameter solenoid coil which serves as both RF transmitter and receiver. The mid-sagittal slice of each brain was acquired in a 4.7 T Varian UNITY INOVA spectrometer with an actively shielded Magnex gradient coil (10 cm inner diameter, 60 g/cm, 100 μs rise time). A fast spin echo sequence with a 1 ms sinc inversion pulse was used for the qMT experiments. Eighteen images with inversion times ranging from 5 ms to 7.9 s were obtained with 2 s constant pre-delay t_d, 8 averages, 16 echoes, 10 ms echo spacing time, 25 mm × 25 mm field of view, 0.8 mm thick slice, and 256 × 256 data matrix. The total imaging time was 2 h. A bi-exponential function of the inversion times (eqn (A1)) was used to fit the data to determine qMT parameters pixel by pixel. The details of qMT parameters determination are given in the Appendix. DTI was performed on the same selected slices with the same spatial resolution and a diffusion weighted spin echo pulse sequence with 1 s repetition time, 4 averages, 38 ms echo time, 13 ms time between gradient pulses, 4 ms diffusion gradient duration, b value of 1.879 ms/μm^2, diffusion sensitizing gradients along six directions (1,1,0), (0,1,1), (1,0,1), (−1,1,0), (0,−1,1), and (1,0,−1), plus a normalizing image with no diffusion gradients. The DTI scan time was 2 h.

Statistical analysis

The Shapiro–Wilk W-test and Lilliefors test were performed to the qMT and DTI data and no evidence of non-normality was found. For each qMT and DTI parameter, statistical differences between control mice and shiverer mice were evaluated using the Student's t-test. The t-value was calculated by the means and standard deviations of each parameter in control/shiverer mice. With the t-value and the known degree of freedom (six control mice and six shiverer mice gave a degree of freedom 10), the probability (p-value) that each parameter is the same in control mice as well as in shiverer mice was determined. The correlation coefficient of the pool size ratio to the radial diffusivity was also calculated by Pearson's correlation coefficient test.

Histology

For examining myelin integrity, 3 μs thick slices matching the DTI and qMT images (mid-sagittal slices) were cut from paraffin embedded tissue and cleared in xylene. The primary

antibody detecting myelin basic protein (MBP, 1:100; Zymed laboratories Inc., South San Francisco, CA, USA) was revealed by avidinbiotin-peroxidase method (Vector Laboratories, Inc. Burlingame, CA, USA). Images were captured with a Photometrics CCD digital camera using MetaMorph image acquisition software (Universal Imaging Corporation, Downington, PA, USA) on a Nikon Eclipse 80i microscope.

RESULTS

Figure 1 is a T_2 weighted spin echo image without diffusion gradients illustrating the mouse brain anatomy in the mid-sagittal slice. The regions of interest (ROI) of white and gray matter for the quantitative study are also shown in this figure. Other ROIs which we have analyzed but not shown here include: the cerebellum white matter (parameter measurements are overwhelmed by partial volume effects) and the subcortical gray matter (measured parameters are similar to those from the presented cortical gray matter). Representative qMT, DTI, and immunohistochemistry maps for the mid-sagittal slice of one control and one shiverer mice are presented to demonstrate the consistent findings among different methods (Fig. 2). Significantly reduced intensity in the pool size ratio map and the markedly reduced contrast (between white and gray matter) in the radial diffusivity map are in close agreement with the loss of intensity in the immunohistochemical staining of MBP when comparing the corpus callosum from the shiverer with that of the control mice. Given the almost complete absence of myelin sheath in the shiverer mice CNS white matter, we did not attempt a quantitative estimation of myelin content in the histological studies.

Quantitative magnetization transfer imaging

Data from the SIR-FSE pulse sequence were fitted by the bi-exponential eqn (A1) and qMT parameters were calculated pixel-by-pixel from eqn (A3). The resulting pool size ratio, fast recovery rate, and slow recovery rate of both white and gray matter ROIs of each individual mouse were averaged and listed in Table 1. Figure 3 shows the comparison of the pool size ratio between the white and gray matter for the six control and six shiverer mice. The pool size ratio of control mice white matter is about 30% higher than that of gray matter; the pool size ratio of shiverer mice white matter is almost the same as that of gray matter. In addition, as shown in Fig. 4, the white matter pool size ratio of control mice is about 25% higher than the white matter pool size ratio of shiverer mice ($p = 0.002$); the pool size ratio of gray matter is roughly the same (~5% difference, smaller than the uncertainty scale; $p = 0.14$) for both control and shiverer mice.

There is nearly no difference ($p = 0.58$) for the white matter fast rates when comparing the control and shiverer mice. There is no gray matter fast rates difference ($p = 0.98$) between the control and shiverer mice as well. The white matter slow rate is slightly higher than the gray matter slow rate for the control mice, while the slow rate is higher in the gray matter and lower in the white matter for the shiverer mice. There is about 8% difference ($p = 0.0002$) of slow rates between control and shiverer mice white matter, and no difference ($p = 0.52$) of slow rates between control and shiverer mice gray matter.

Diffusion tensor imaging

Diffusion weighted images data were analyzed to derive the directional diffusivity maps. The resulting radial and axial diffusivities are listed in Table 1. As shown in Fig. 4, the radial diffusivity in the control mice white matter is about 25% less than that in the shiverer mice white matter ($p = 0.01$); the axial diffusivity in the control mice white matter is almost indistinguishable (about 5% difference, smaller than the uncertainty scale; $p = 0.27$) from that in the shiverer mice white matter; the diffusivity in the gray matter is always about the same for control and shiverer mice (radial: $p = 0.78$; axial: $p = 0.91$). The calculated

principle diffusion direction in the white matter (corpus callosum) is always perpendicular to the mid-sagittal plane, the same for both control and shiverer mice.

Correlation of qMT and DTI parameters

Figure 5 is a scatter plot for the qMT measured pool size ratio and DTI measured radial diffusivity for all pixels in all mice. In white matter, the results from the control and shiverer mice are distinct in the scatter plot; in gray matter, the results from the control and shiverer mice are similar. For the pool size ratio and radial diffusivity, a significant correlation ($r = -0.57$, $p = 0.025$) was found in the white matter when using the average for each mouse as a data point (subplot in Fig. 5). No significant correlation was found when control and shiverer mice groups were considered individually.

DISCUSSION

Control vs. shiverer

Shiverer mouse is a well-characterized model of CNS dysmyelination (29,30). Our results suggest that the qMT measured pool size ratio may be a valid maker for non-invasive evaluation of myelin in shiverer mouse brain. The measured pool size ratio in the control mice white matter (corpus callosum) is much higher (about 25%) than that in the shiverer mice white matter, while the pool size ratio in the control mice gray matter is similar to that in the shiverer mice gray matter, indicating that the difference in the pool size ratio is caused by the difference of myelin integrity. Likewise, the resistance to water diffusion in the perpendicular direction of axon fibers is strongly affected by the surrounding myelin sheath, and published results (9,26) suggest that the radial diffusivity may reflect myelin integrity. In our experiments, we found that the radial diffusivity in the control mice white matter is less (about 25%) than that in the shiverer mice white matter. The selection of corpus callosum in the mid-sagittal slice as the ROI for white matter also reduces the possibility of contaminated radial diffusivity measurements by crossing fibers, as the corpus callosum in the mid-sagittal slice is the region in which radial diffusivity is most specific to myelination (33). There is no difference for the radial diffusivity in the gray matter between the two groups of mice. These DTI results correlate well with the qMT results. The percentage differences in the pool size ratio and in the radial diffusivity between control and shiverer mice white matter are similar. Though theoretically all mice white matter may be grouped into two distinct states, control and shiverer, the individual differences for the mice may still validate the correlation analysis, and in this case the relatively large correlation coefficient ($r = -0.57$) and statistically significant p-values ($p = 0.025$) are an indication that the pool size ratio is correlated with radial diffusivity. The percentage difference in macromolecular proton pool size ratios between control and shiverer is smaller than that measured in shiverer mice spinal cord (32), which may reflect differences between brain and spinal cord, sample preparation, or qMT acquisition method. The difference (about 8%) in the observed recovery rate (slow recovery rate, the reciprocal of conventional T_1) between control and shiverer mice white matter is much smaller than the difference we observed in qMT and DTI parameters, suggesting that both qMT and DTI are superior to T_1 weighted images or T_1 maps in terms of sensitivity to myelin changes. Our qMT results agree well with the histology results (Fig. 2), though quantitative correlation with histology is still needed to confirm whether qMT can be indeed a valid marker for myelin.

White matter vs. gray matter

While the lipids in myelin are a conduit for spin exchange between the free water and macromolecules (34,35), myelin is not the only microstructure in the mouse brain that contributes to the pool size ratio. Gray matter does not have significant myelin, but still has a non-zero pool size ratio. However, the lack of gray/white matter contrast in the pool size

ratio map of the shiverer mouse in Fig. 2, and the corresponding values listed in Table 1 support the view that it is myelin alone that accounts for the pool size ratio difference between gray and white matter in normal mice. That is, our findings indicate that microstructures other than myelin (e.g. axon fibers) in the white matter have similar qMT properties as microstructures in gray matter. On the other hand, myelin is not the only underlying mechanism influencing the radial diffusion in the gray and white matter. Shiverer mice white matter has no myelin but only has half the radial diffusivity of gray matter (Table 1). That is, even without myelin, white and gray matter are differentiated by radial diffusivity, but not the pool size ratio. One possible practical benefit of this effect is that a pool size ratio map may indicate demyelinated white matter regions without requiring knowledge of normal white matter values.

Other qMT and DTI parameters

The fast recovery rate and the slow recovery rate of mouse brains were also obtained from qMT results (Table 1). The fast recovery rate, which is approximately equal to the MT exchange rate from the macromolecular protons to free water protons, is not differentiated between the control and shiverer mice. This result is similar to the result of a qMT study of demyelinated sciatic nerve (36), in which the exchange rate appeared to be independent of demyelination. It is also similar to the results from human brain in which the exchange rates from macromolecular protons to free water protons are not differentiated between white and gray matter (37). The slow recovery rate, which is the reciprocal of the apparent T_1 relaxation time, is higher in control mice white matter than that in the dysmyelinated shiverer mice, in agreement with previous results in peripheral nerves (36). However, the differences in these parameters between white and gray matter are relatively small, likely due to fixation effects as discussed below. The axial diffusivity in white matter is not changed between control and shiverer mice, which agrees well with previous results (9,26), and indicates that axon fibers are still intact in shiverer mice. Furthermore, both axial and radial diffusivities in gray matter are also very similar in control and shiverer mice. These results are expected for our animal model, since the only major difference between control and shiverer mice is the myelin sheath in white matter, and there is no substantial structural difference for gray matter.

The effects of formalin fixation

We have demonstrated that both qMT and DTI may be capable of characterizing myelin content in the *ex vivo* mouse brain. Also determined but not shown is that these results did not change when we measured the same sample at 2 weeks after perfusion (compared to measurements at 1 week after perfusion), indicating that our 1 week formalin/PBS fixation procedure was sufficient to reach a steady-state condition. Our samples were imaged shortly after transfer from the formalin/PBS solution to PBS with a brief PBS washing. Some studies have observed changes in the relaxation and diffusion properties of specific samples after 12 h of PBS washing (38). The short-term effect of switching from fixation solution to PBS was not measured in our study. Published results suggest that the directional diffusivities *ex vivo* are smaller than those *in vivo*, but measures of anisotropy do not change (39). Our DTI results are consistent with these *ex vivo* results. A recent publication compared the qMT and DTI results in WMLs and NAWM in postmortem MS brain before and after formalin fixation, and suggested that useful conclusions about *in vivo* changes may be inferred from data acquired using fixed tissues (40). Their results show that the pool size ratio difference and water diffusivity differences between the NAWM and the demyelinated WML are preserved after fixation. We do not have a direct comparison of *ex vivo* (before and after fixation) and *in vivo* qMT parameters on the same animal model. Nevertheless, our *ex vivo* qMT results in this study differ from *in vivo* measurements in ferret brain acquired using the same pulse sequence (20), though these differences could be due to the change in

animal model in addition to fixation effects. For all parameters, the *ex vivo* qMT results have smaller parameter differences between gray and white matter than their *in vivo* counterparts, possibly due to the combined effects of death and fixation of the animal overwhelming inherent tissue characteristics.

Multi-contrast quantitative MRI methods for myelin measurement

Many quantitative measurements by MRI are sensitive to myelin. However, other biological microstructures (such as axon fibers) also affect most of those measurements. Multiple contrast MRI experiments were used by many researchers to investigate the specificity of certain MRI parameters to myelin. For example, multi-component T_1 and T_2 measurements were performed together with MTR measurements to show that the change of MTR cannot be attributed solely to the change of myelination (4,5). On the other hand, the combination of T_1, T_2, and MT contrast does increase the myelin specificity in a cuprizone mouse model which has selective and reversible demyelination with little or no axonal damage. The combination of these contrasts can separate normal, demyelinated, and remyelinated white matter 95% of the time, better than individual measurements (41).

When compared to MTR, qMT parameters increase the specificity to myelin by characterizing the intrinsic properties of MT. However, the specificity of qMT parameters to demyelination still needs further investigation. The roles of axonal degeneration, inflammation, and edema in the pool size ratio measurements were not addressed in this study. Those pathologies may affect the qMT demyelination measurements, as indicated by some multiple contrast quantitative MRI methods. For example, the qMT pool size ratio has been correlated to the myelin water fraction in multiple component T_2 measurements (42,43) investigating specificity to myelin. It was found that both parameters reflect the same thing (most likely myelin) to a great extent, but inflammation (43) may be difficult to distinguish from demyelination by pool size ratio measurements alone.

In this paper, we correlated the pool size ratio in qMT with the radial diffusivity in DTI to demonstrate the sensitivity of the pool size ratio to myelin by choosing two kinds of animals (shiverer and control mice) which are mainly differentiated by myelin content, without the involvement of other white matter disease pathologies, such as axonal degeneration, inflammation, and edema. Our results indicate a similar sensitivity for the radial diffusivity and the pool size ratio to changes in myelin between control and shiverer mice. While both these measurements are sensitive to myelin content, the mechanism of this sensitivity varies and may therefore reflect differently on subtle changes in pathology. The pool size ratio is determined by the lipids in myelin which are a conduit for spin exchange between the free water and macromolecules; the radial diffusivity is directly affected by themyelin sheath inhibition of water diffusion. Although not addressed in this study, the short T_2 spectrum from multiple exponential T_2 (MET2) method is also likely caused by myelin lipids increasing the associated water relaxation rate. The relative merits, sensitivities, and specificities of these three measures are interesting topics for further quantitative MRI studies on myelin.

CONCLUSION

We applied a qMT imaging technique on *ex vivo* shiverer mouse brain, and compared these results with DTI and histology. Our results suggest that the pool size ratio and the radial diffusivity may be correlated. Both of them may be potential non-invasive biomarkers for myelin detection.

Acknowledgments

This research was supported by the NIH (R01EB001452, R01NS047592, R01NS054194) and NMSS (RG 3864, CA 1012).

Contract/grant sponsor: NIH; contract/grant numbers: R01EB001452; R01NS 047592; R01NS054194.

Contract/grant sponsor: NMSS; contract/grant numbers: RG 3864; CA 1012.

Abbreviations used

CW	continuous wave
DTI	diffusion tensor imaging
MBP	myelin basic protein
MS	multiple sclerosis
MT	magnetization transfer
MTR	magnetization transfer ratio
NAWM	normal appearing white matter
PBS	phosphate-buffered saline
qMT	quantitative magnetization transfer
SIR-FSE	selective inversion recovery fast-spin-echo
WML	white matter lesion

REFERENCES

1. Trapp BD, Bo L, Mork S, Chang A. Pathogenesis of tissue injury in MS lesions. J. Neuroimmunol. 1999; 98(1):49–56. [PubMed: 10426362]
2. Steinman L. Multiple sclerosis: a coordinated immunological attack against myelin in the central nervous system. Cell. 1996; 85(3):299–302. [PubMed: 8616884]
3. Miller DH, Grossman RI, Reingold SC, McFarland HF. The role of magnetic resonance techniques in understanding and managing multiple sclerosis. Brain. 1998; 121:3–24. [PubMed: 9549485]
4. Does MD, Beaulieu C, Allen PS, Snyder RE. Multi-component T-1 relaxation and magnetisation transfer in peripheral nerve. Magn. Reson. Imaging. 1998; 16(9):1033–1041. [PubMed: 9839987]
5. Gareau PJ, Rutt BK, Karlik SJ, Mitchell JR. Magnetization transfer and multicomponent T2 relaxation measurements with histopathologic correlation in an experimental model of MS. J. Magn. Reson. Imaging. 2000; 11(6):586–595. [PubMed: 10862056]
6. Tozer D, Ramani A, Barker GJ, Davies GR, Miller DH, Tofts PS. Quantitative magnetization transfer mapping of bound protons in multiple sclerosis. Magn. Reson. Med. 2003; 50(1):83–91. [PubMed: 12815682]
7. Stanisz GJ, Kecojevic A, Bronskill MJ, Henkelman RM. Characterizing white matter with magnetization transfer and T-2. Magn. Reson. Med. 1999; 42(6):1128–1136. [PubMed: 10571935]
8. Sled JG, Pike GB. Quantitative imaging of magnetization transfer exchange and relaxation properties in vivo using MRI. Magn. Reson. Med. 2001; 46(5):923–931. [PubMed: 11675644]
9. Song SK, Sun SW, Ramsbottom MJ, Chang C, Russell J, Cross AH. Dysmyelination revealed through MRI as increased radial (but unchanged axial) diffusion of water. Neuroimage. 2002; 17(3): 1429–1436. [PubMed: 12414282]
10. Mackay A, Whittall K, Adler J, Li D, Paty D, Graeb D. In-vivo visualization of myelin water in brain by magnetic resonance. Magn. Reson. Med. 1994; 31(6):673–677. [PubMed: 8057820]

11. Laule C, Vavasour IM, Moore GRW, Oger J, Li DKB, Paty DW, MacKay AL. Water content and myelin water fraction in multiple sclerosis—a T-2 relaxation study. J. Neurol. 2004; 251(3):284–293. [PubMed: 15015007]
12. Does MD, Snyder RE. Multiexponential T-2 relaxation in degenerating peripheral nerve. Magn. Reson. Med. 1996; 35(2):207–213. [PubMed: 8622585]
13. Berry I, Barker GJ, Barkhof F, Campi A, Dousset V, Franconi JM, Gass A, Schreiber W, Miller DH, Tofts PS. A multicenter measurement of magnetization transfer ratio in normal white matter. J. Magn. Reson. Imaging. 1999; 9(3):441–446. [PubMed: 10194715]
14. Sled JG, Levesque I, Santos AC, Francis SJ, Narayanan S, Brass SD, Arnold DL, Pike GB. Regional variations in normal brain shown by quantitative magnetization transfer imaging. Magn. Reson. Med. 2004; 51(2):299–303. [PubMed: 14755655]
15. Sled JG, Pike GB. Quantitative interpretation of magnetization transfer in spoiled gradient echo MRI sequences. J. Magn. Reson. 2000; 145(1):24–36. [PubMed: 10873494]
16. Ramani A, Dalton C, Miller DH, Tofts PS, Barker GJ. Precise estimate of fundamental in-vivo MT parameters in human brain in clinically feasible times. Magn. Reson. Imaging. 2002; 20(10):721–731. [PubMed: 12591568]
17. Henkelman RM, Huang XM, Xiang QS, Stanisz GJ, Swanson SD, Bronskill MJ. Quantitative interpretation of magnetization transfer. Magn. Reson. Med. 1993; 29(6):759–766. [PubMed: 8350718]
18. Ropele S, Seifert T, Enzinger C, Fazekas F. Method for quantitative imaging of the macromolecular 1H fraction in tissues. Magn. Reson. Med. 2003; 49(5):864–871. [PubMed: 12704769]
19. Yarnykh VL. Pulsed Z-spectroscopic imaging of cross-relaxation parameters in tissues for human MRI: theory and clinical applications. Magn. Reson. Med. 2002; 47(5):929–939. [PubMed: 11979572]
20. Gochberg DF, Gore JC. Quantitative magnetization transfer imaging via selective inversion recovery with short repetition times. Magn. Reson. Med. 2007; 57(2):437–441. [PubMed: 17260381]
21. Gochberg DF, Gore JC. Quantitative imaging of magnetization transfer using an inversion recovery sequence. Magn. Reson. Med. 2003; 49(3):501–505. [PubMed: 12594753]
22. Horsfield MA, Lai M, Webb SL, Barker GJ, Tofts PS, Turner R, Rudge P, Miller DH. Apparent diffusion coefficients in benign and secondary progressive multiple sclerosis by nuclear magnetic resonance. Magn. Reson. Med. 1996; 36(3):393–400. [PubMed: 8875409]
23. Horsfield MA, Jones DK. Applications of diffusion-weighted and diffusion tensor MRI to white matter diseases—a review. NMR Biomed. 2002; 15(7–8):570–577. [PubMed: 12489103]
24. Filippi M, Cercignani M, Inglese M, Horsfield MA, Comi G. Diffusion tensor magnetic resonance imaging in multiple sclerosis. Neurology. 2001; 56(3):304–311. [PubMed: 11171893]
25. Sun SW, Liang HF, Le TQ, Armstrong RC, Cross AH, Song SK. Differential sensitivity of in vivo and ex vivo diffusion tensor imaging to evolving optic nerve injury in mice with retinal ischemia. Neuroimage. 2006; 32(3):1195–1204. [PubMed: 16797189]
26. Song SK, Yoshino J, Le TQ, Lin SJ, Sun SW, Cross AH, Armstrong RC. Demyelination increases radial diffusivity in corpus callosum of mouse brain. Neuroimage. 2005; 26(1):132–140. [PubMed: 15862213]
27. Kim JH, Budde MD, Liang HF, Klein RS, Russell JH, Cross AH, Song SK. Detecting axon damage in spinal cord from a mouse model of multiple sclerosis. Neurobiol. Dis. 2006; 21(3):626–632. [PubMed: 16298135]
28. Song SK, Sun SW, Ju WK, Lin SJ, Cross AH, Neufeld AH. Diffusion tensor imaging detects and differentiates axon and myelin degeneration in mouse optic nerve after retinal ischemia. Neuroimage. 2003; 20(3):1714–1722. [PubMed: 14642481]
29. Privat A, Jacque C, Bourre JM, Dupouey P, Baumann N. Absence of the major dense line in myelin of the mutant mouse shiverer. Neurosci. Lett. 1979; 12(1):107–112. [PubMed: 460693]
30. Inoue Y, Nakamura R, Mikoshiba K, Tsukada Y. Fine structure of the central myelin sheath in the myelin deficient mutant shiverer mouse, with special reference to the pattern of myelin formation by oligodendroglia. Brain Res. 1981; 219(1):85–94. [PubMed: 7260630]

31. Griffiths I, Klugmann M, Anderson T, Yool D, Thomson C, Schwab MH, Schneider A, Zimmermann F, McCulloch M, Nadon N, Nave KA. Axonal swellings and degeneration in mice lacking the major proteolipid of myelin. Science. 1998; 280(5369):1610–1613. [PubMed: 9616125]
32. Portnoy S, Stanisz GJ. Modeling pulsed magnetization transfer. Magn. Reson. Med. 2007; 58(1): 144–155. [PubMed: 17659607]
33. Larvaron P, Boespflug-Tanguy O, Renou JP, Bonny JM. In vivo analysis of the post-natal development of normal mouse brain by DTI. NMR Biomed. 2007; 20(4):413–421. [PubMed: 17120295]
34. Koenig SH. Cholesterol of myelin is the determinant of gray-white contrast in MRI of brain. Magn. Reson. Med. 1991; 20(2):285–291. [PubMed: 1775053]
35. Koenig SH, Brown RD 3rd, Spiller M, Lundbom N. Relaxometry of brain: why white matter appears bright in MRI. Magn. Reson. Med. 1990; 14(3):482–495. [PubMed: 2355830]
36. Odrobina EE, Lam TY, Pun T, Midha R, Stanisz GJ. MR properties of excised neural tissue following experimentally induced demyelination. NMR Biomed. 2005; 18(5):277–284. [PubMed: 15948233]
37. Sinson G, Bagley LJ, Cecil KM, Torchia M, McGowan JC, Lenkinski RE, McIntosh TK, Grossman RI. Magnetization transfer imaging and proton MR spectroscopy in the evaluation of axonal injury: correlation with clinical outcome after traumatic brain injury. Am. J. Neuroradiol. 2001; 22(1):143–151. [PubMed: 11158900]
38. Thelwall PE, Shepherd TM, Stanisz GJ, Blackband SJ. Effects of temperature and aldehyde fixation on tissue water diffusion properties, studied in an erythrocyte ghost tissue model. Magn. Reson. Med. 2006; 56(2):282–289. [PubMed: 16841346]
39. Sun SW, Neil JJ, Song SK. Relative indices of water diffusion anisotropy are equivalent in live and formalin-fixed mouse brains. Magn. Reson. Med. 2003; 50(4):743–748. [PubMed: 14523960]
40. Schmierer K, Wheeler-Kingshott CA, Tozer DJ, Boulby PA, Parkes HG, Yousry TA, Scaravilli F, Barker GJ, Tofts PS, Miller DH. Quantitative magnetic resonance of postmortem multiple sclerosis brain before and after fixation. Magn. Reson. Med. 2008; 59(2):268–277. [PubMed: 18228601]
41. Merkler D, Boretius S, Stadelmann C, Ernsting T, Michaelis T, Frahm J, Bruck W. Multicontrast MRI of remyelination in the central nervous system. NMR Biomed. 2005; 18(6):395–403. [PubMed: 16086436]
42. Tozer DJ, Davies GR, Altmann DR, Miller DH, Tofts PS. Correlation of apparentmyelin measures obtained in multiple sclerosis patients and controls from magnetization transfer and multicompartmental T-2 analysis. Magn. Reson. Med. 2005; 53(6):1415–1422. [PubMed: 15906291]
43. Stanisz GJ, Webb S, Munro CA, Pun T, Midha R. MR properties of excised neural tissue following experimentally induced inflammation. Magn. Reson. Med. 2004; 51(3):473–479. [PubMed: 15004787]
44. Gochberg DF, Kennan RP, Gore JC. Quantitative studies of magnetization transfer by selective excitation and T-1 recovery. Magn. Reson. Med. 1997; 38(2):224–231. [PubMed: 9256101]
45. Gochberg DF, Kennan RP, Robson MD, Gore JC. Quantitative imaging of magnetization transfer using multiple selective pulses. Magn. Reson. Med. 1999; 41(5):1065–1072. [PubMed: 10332891]
46. Basser PJ, Pierpaoli C. Microstructural and physiological features of tissues elucidated by quantitative-diffusion-tensor MRI. J. Magn. Reson. B. 1996; 111(3):209–219. [PubMed: 8661285]

APPENDIX

THE SIR-FSE SEQUENCE

SIR-FSE is a recently developed qMT imaging method (20,21). This technique uses a fast spin echo pulse sequence with a preceding 180° inversion pulse. A series of inversion times are used to model the transient signal of the magnetization recovery after the inversion pulse. A constant pre-delay time t_d (the time delay after the fast spin echo acquisition in each

repetition), instead of a constant repetition time TR, is used to maximize the efficiency of SIR-FSE (20). In the SIR-FSE model, there are three essential qMT parameters: the pool size ratio, which is the ratio of the size of the immobile macromolecular protons to the size of the free water protons; the fast recovery rate, which is the recovery rate of the inverted magnetization at short inversion times; and the slow recovery rate, which is the recovery rate of the inverted magnetization at long inversion times, and is the reciprocal of the conventional T_1 relaxation time.

For a two-pool system (such as the immobile macromolecular and free water proton pools measured in brain tissue), the recovery of the inverted free pool magnetization after the inversion pulse is

$$\frac{M_{\mathrm{f}}(t)}{M_{\mathrm{f}\infty}} = b_{\mathrm{f}}^{+}\exp(-R_1^{+}t) + b_{\mathrm{f}}^{-}\exp(-R_1^{-}t) + 1 \quad \text{(A1)}$$

where

$$\begin{aligned} 2R_1^{\pm} &= R_{1\mathrm{f}} + R_{1\mathrm{m}} + k_{\mathrm{fm}} + k_{\mathrm{mf}} \\ &\pm \sqrt{(R_{1\mathrm{f}} - R_{1\mathrm{m}} + k_{\mathrm{fm}} - k_{\mathrm{mf}})^2 + 4k_{\mathrm{fm}}\, k_{\mathrm{mf}}} \end{aligned} \quad \text{(A2)}$$

R_1^{-} and R_1^{+} are the slow and fast recovery rates, respectively. The subscripts f and m refer to the free and macromolecular proton pools, respectively. $M_{\mathrm{f}}(t)$ and $M_{\mathrm{m}}(t)$ are the longitudinal magnetizations with equilibrium values $M_{\mathrm{f}\infty}$ and $M_{\mathrm{m}\infty}$. $R_{1\mathrm{f}}$ and $R_{1\mathrm{m}}$ are the longitudinal relaxation rates of the free and macromolecular protons when there is no magnetization transfer between them. k_{fm} is the magnetization exchange rate from the free pool to the macromolecular pool, k_{mf} is the rate from the macromolecular pool to the free pool, and $k_{\mathrm{fm}}/k_{\mathrm{mf}}$ is equal to the pool size ratio ($p_{\mathrm{m}}/p_{\mathrm{f}}$).

k_{mf} is usually much larger than any other rate, and a Taylor expansion gives the approximations (20):

$$k_{\mathrm{mf}} \approx R_1^{+} \text{ and } \frac{p_{\mathrm{m}}}{p_{\mathrm{f}}} \approx \frac{b_{\mathrm{f}}^{+}}{(b_{\mathrm{f}}^{+} + b_{\mathrm{f}}^{-} + 1 - S_{\mathrm{m}}(1 - e^{-R_1^{-}t_d}))} \quad \text{(A3)}$$

In the experiments, $R_1^{+}, R_1^{-}, b_{\mathrm{f}}^{+}$, and b_{f}^{-} are determined by fitting eqn (A1) to the measured images, where t is the varied inversion time, and k_{mf} and $p_{\mathrm{m}}/p_{\mathrm{f}}$ are determined from eqn (A3), where t_{d} is the constant pre-delay and S_{m} is the simulated saturation effect of the rf pulse (0.41 ± 0.11 for a 1 ms sinc inversion pulse on a solid pool with a Gaussian lineshape and a T_2 between 10 and 20 μs, calculated as in previous studies (44,45)). Being an on-resonance method, the results have little dependence on the assumed lineshape, as discussed in previous publications (21).

DIRECTIONAL DIFFUSIVITIES DERIVED BY DIFFUSION TENSOR IMAGING

The diffusion tensor (**D**) can be derived according to eqn (A4), where S is the diffusion-weighted signal, S_0 is the signal with diffusion weighting factor $b = 0$, and **n** is the encoding direction (46). The resulting tensor element maps are used to derive eigenvalues (λ_1, λ_2, λ_3) of the diffusion tensor by matrix diagonalization. On a pixel-by-pixel basis, quantitative

indices including axial diffusivity ($\lambda_{\parallel}$) and radial diffusivity ($\lambda_{\perp}$), defined by the eqns (A5,A6), are derived using a software written in Matlab (MathWorks, Natick, MA, USA)

$$S = S_0 \exp(-\mathrm{b} \cdot \mathbf{n} \cdot \mathbf{D} \cdot \mathbf{n}^{\mathrm{T}}) \sqrt{a^2 + b^2} \quad \text{(A4)}$$

$$\lambda_{\parallel} = \lambda_1 \quad \text{(A5)}$$

$$\lambda_{\perp} = 0.5 \times (\lambda_2 + \lambda_3) \quad \text{(A6)}$$

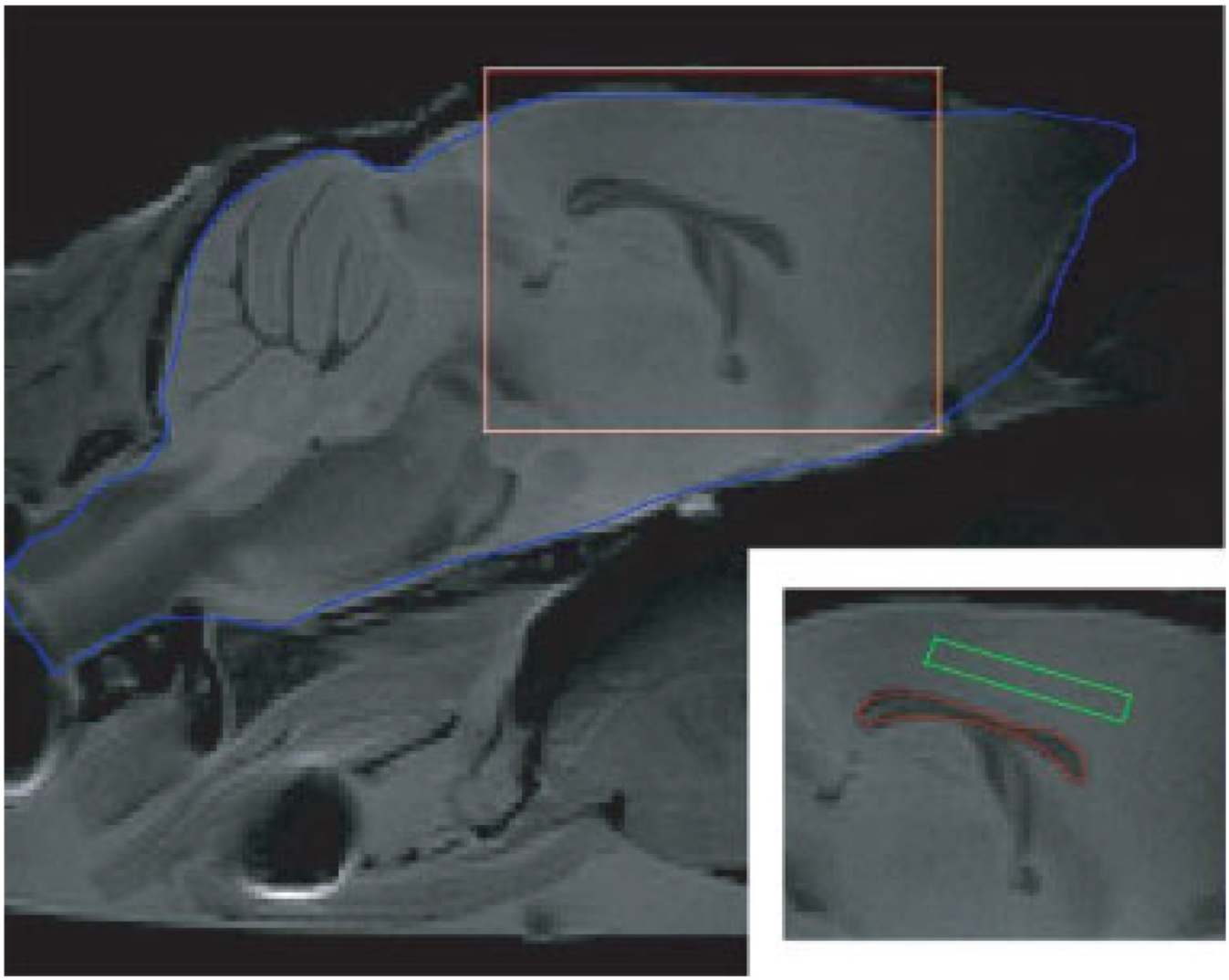

Figure 1.
The T_2 weighted MRI for a mid-sagittal slice of a fixed control mouse head. The brain of the mouse is sketched by the blue line. The subfigure in the bottom right corner shows the rectangular area in the main figure, and with the ROIs for white matter (red) and gray matter (green) sketched. For each mouse, we chose the whole corpus callosum (50–60 pixels, without boundary pixels) as the ROI of white matter, and chose a rectangle (about 50–60 pixels) in the cortical gray matter superior to the corpus callosum as the ROI of gray matter.

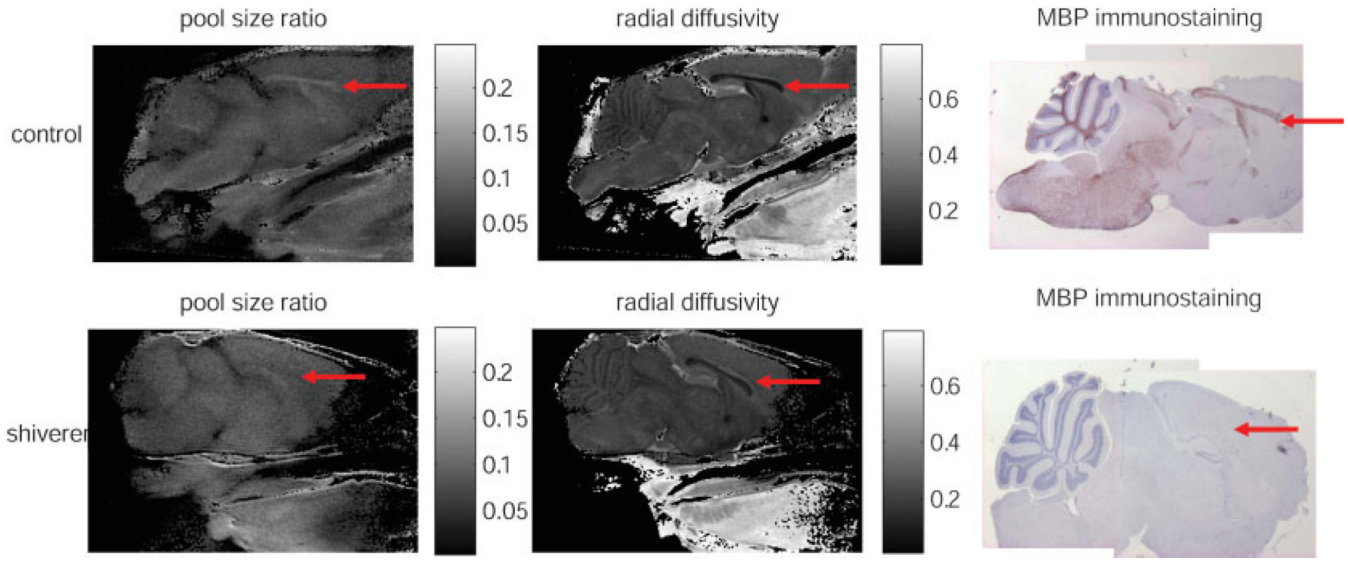

Figure 2.

The pool size ratio (left), the radial diffusivity (center), and the MBP staining (right) for the control (top row) and shiverer mice (bottom row) are compared. The red arrow inside each image points to the corpus callosum in the mouse brain. In the qMT and MBP maps, the corpus callosum is visible for the control, but not for the shiverer mouse.

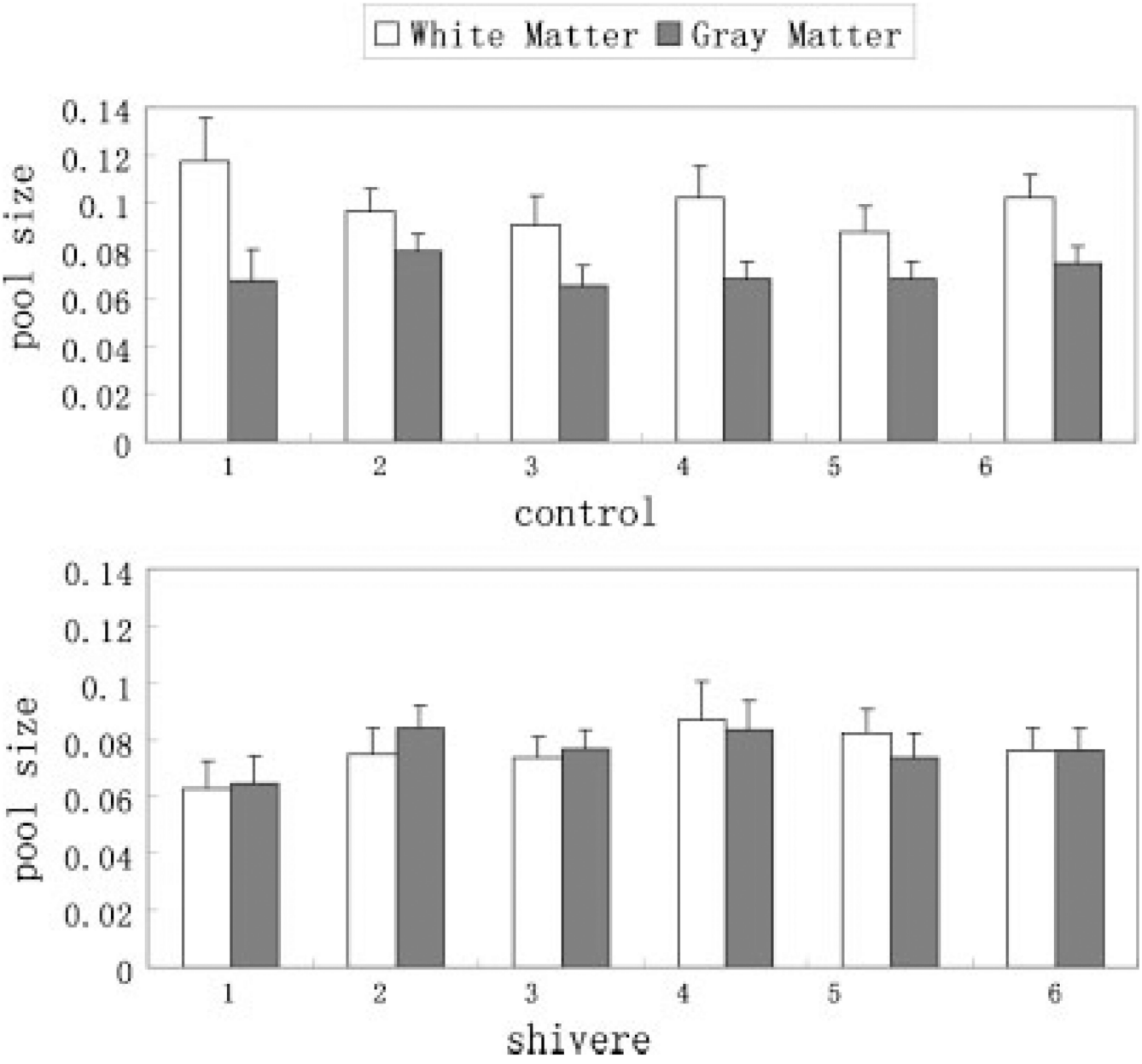

Figure 3.

Comparison of the pool size ratio in the white matter to that in the gray matter for all control (white matter: 0.099 ± 0.011, gray matter: 0.071 ± 0.005) and shiverer (white matter: 0.076 ± 0.008, gray matter: 0.076 ± 0.007) mice. The error bars represent the pixel-wise standard deviations in the ROIs. The pool size ratio in the white matter is higher than that in the gray matter for the control mice, while it is about the same for the shiverer mice. This figure is available in colour online at www.interscience.wiley.com/journal/nbm

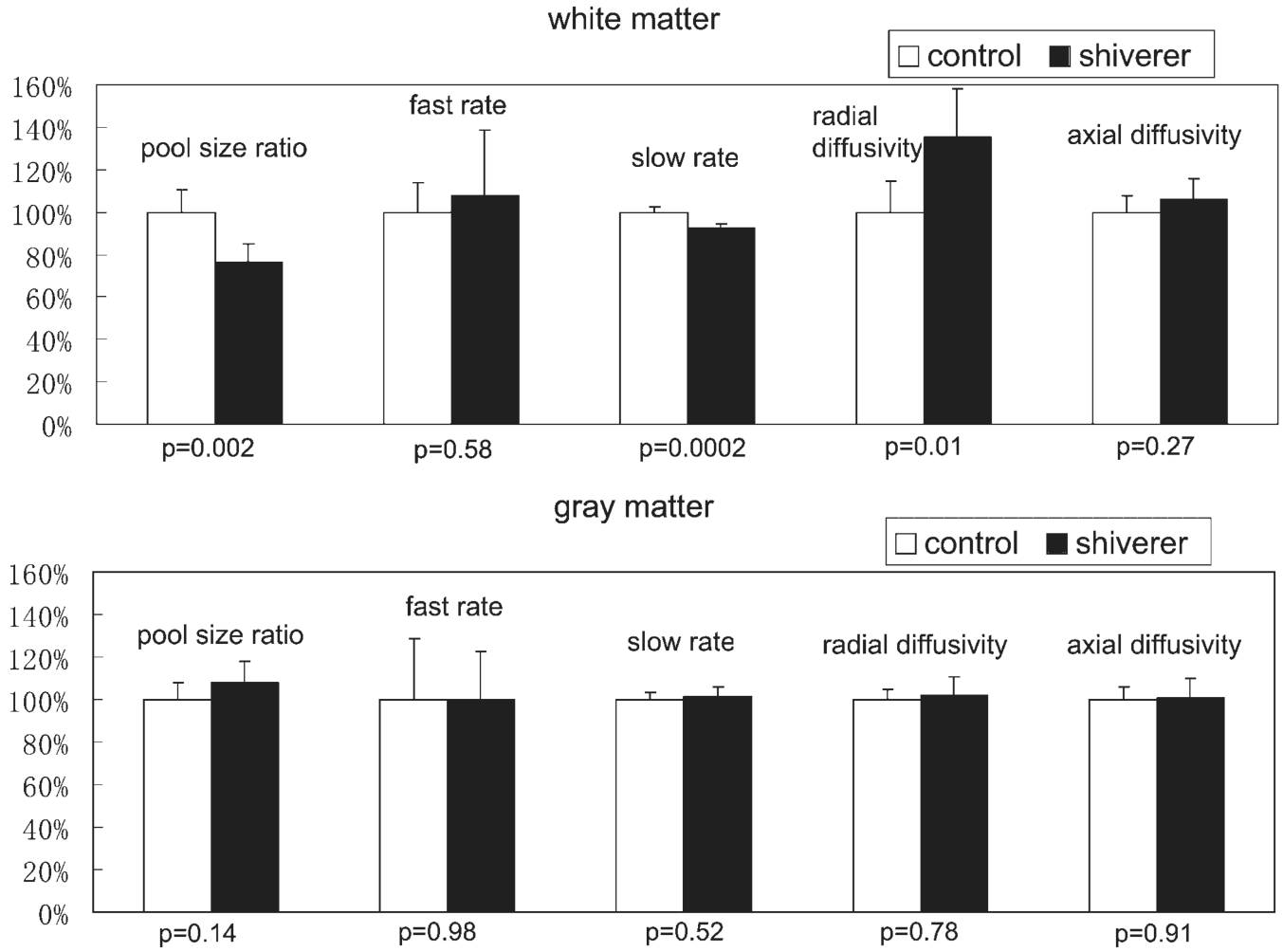

Figure 4.

The percentage differences of qMT and DTI parameters between control mice and shiverer mice. The parameters for control mice were set to 100%. The error bars represent the mouse-wise standard deviations. The *p*-values for statistical significance are also listed on the figure. The pool size ratio and radial diffusivity are different between the control and shiverer mice in the white matter, while they are similar in the gray matter.

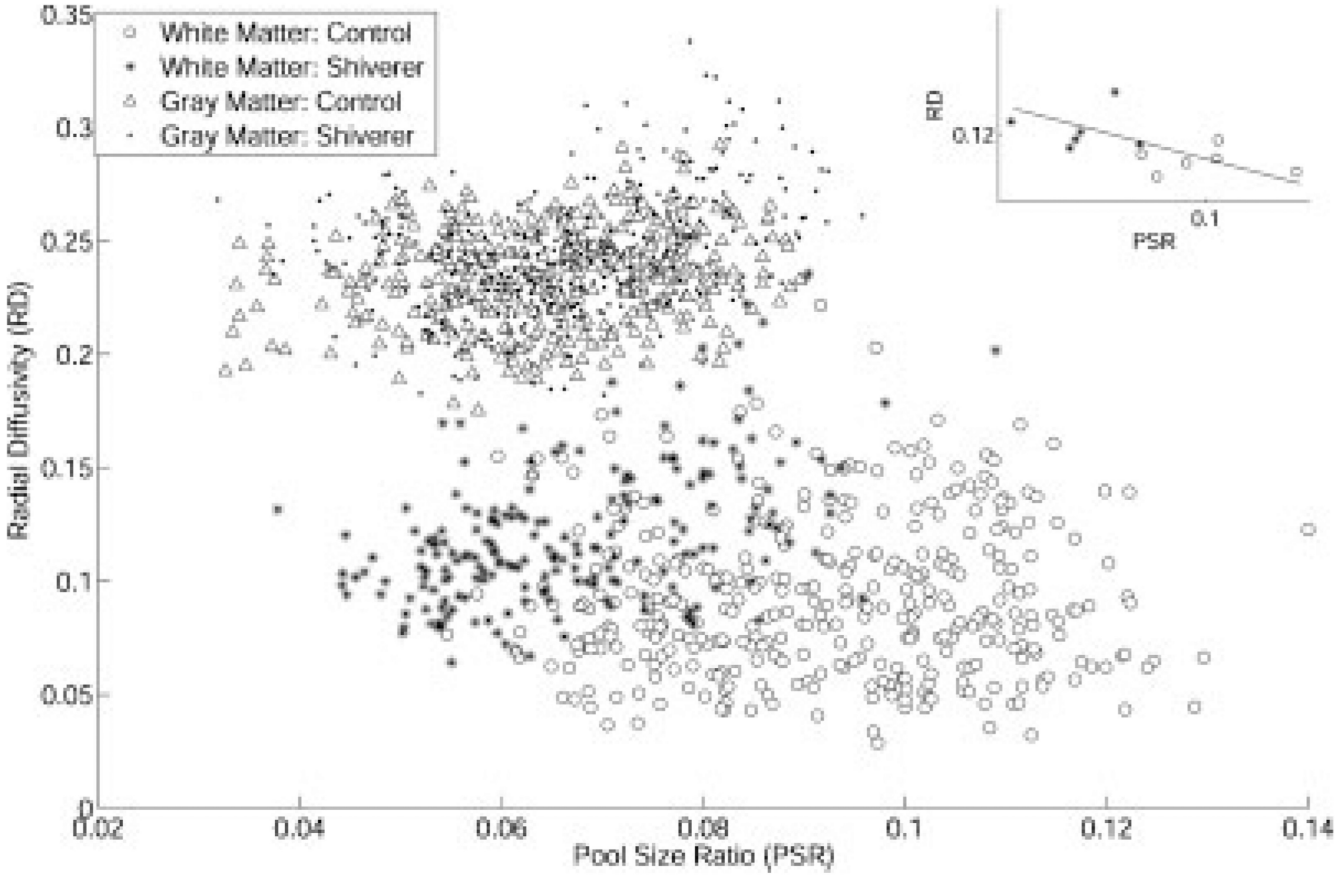

Figure 5.

The scatter plot for the measured pool size ratio and radial diffusivity for all ROI pixels. In the white matter, the control mice pixels were separated from the shiverer mice pixels by higher pool size ratio and smaller radial diffusivity; in the gray matter, the control mice pixels are not separated from the shiverer mice pixels. The subplot shows the correlation ($r = -0.57$, $p = 0.025$) between the pool size ratio and radial diffusivity in the white matter when the average data of each mouse is used as a data point.

Table 1

qMT and DTI parameters

			Control mice (mean ± SD)	Shiverer mice (mean ± SD)	*p*-value
QMT	Pool size ratio	White matter	0.099 ± 0.011	0.076 ± 0.008	0.002
		Gray matter	0.071 ± 0.005	0.076 ± 0.007	0.14
	Fast rate (s^{-1})	White matter	27 ± 4	29 ± 8	0.58
		Gray matter	29 ± 8	28 ± 6	0.98
	Slow rate (s^{-1})	White matter	1.10 ± 0.03	1.02 ± 0.02	0.0002
		Gray matter	1.05 ± 0.04	1.07 ± 0.05	0.52
DTI	Radial diffusivity ($\mu m^2/ms$)	White matter	0.09 ± 0.01	0.12 ± 0.02	0.01
		Gray matter	0.23 ± 0.01	0.24 ± 0.02	0.78
	Axial diffusivity ($\mu m^2/ms$)	White matter	0.40 ± 0.03	0.42 ± 0.04	0.27
		Gray matter	0.31 ± 0.02	0.31 ± 0.03	0.91

The *p*-value represents the statistically significant difference calculated by *t*-test.

NMR Biomed. Author manuscript; available in PMC 2013 July 15.